Structural diversity and topological property of I-based two-dimensional inorganic molecular crystals

Zhili Zhu [1,5,*] Jinhua Gu,[1] Jiaqing Gao,[2] Weiguang Chen,[3] Chunyao Niu,[1] Ping Cui [2,†] Yu Jia,[1,4,5,‡] and Zhenyu Zhang[2,5]

[1]*Key Laboratory of Materials Physics of Ministry of Education, School of Physics and Microelectronics, Zhengzhou University, Zhengzhou 450052, China*

[2]*International Center for Quantum Design of Functional Materials (ICQD), Hefei National Research Center for Physical Sciences at the Microscale, University of Science and Technology of China, Hefei, Anhui 230026, China*

[3]*College of Physics and Electronic Engineering, Zhengzhou Normal University, Zhengzhou, Henan 450044, China*

[4]*Key Laboratory for Special Functional Materials of Ministry of Education, School of Materials Science and Engineering, Henan University, Kaifeng, Henan 475001, China*

[5]*Institute of Quantum Materials and Physics, Henan Academy of Science, Henan 450046, China*

(Received 24 April 2023; revised 1 July 2023; accepted 28 August 2023; published 6 September 2023)

Two-dimensional inorganic molecular crystals (2D IMCs) consisting of compound molecules are emerging as a new branch of the 2D materials family. Based on first-principles calculations, here we propose a 2D IMC class assembled from diatomic molecules whose building blocks are derived from a single element, iodine. We reveal that 2D monolayers of halogen-bonded I_2 molecules can be stabilized with distinct structures of α-I, β-I, and γ-I, and these allotropes are collectively named iodene. Intriguingly, the intermolecular angle between two neighboring I_2 units demonstrate magic angles of 90°, 120°, and 180° for α-I, β-I, and γ-I, respectively, which serves as a degree of freedom to modulate the structural and electronic properties of iodene monolayers. The γ-I behaves as a quantum spin Hall insulator with a band gap of 0.18 eV, which offers a candidate for potential topological 2D IMCs. The α- and β-I phases demonstrate trivial semiconductors with gaps of 2.30 and 1.94 eV. These findings broaden the scope of 2D IMCs stabilized by halogen bonding, with appealing application potentials in molecular physics and optoelectronics.

DOI: 10.1103/PhysRevB.108.115409

I. INTRODUCTION

Since the exfoliation of graphene, two-dimensional (2D) materials have attracted tremendous research interest due to their intriguing emergent properties that can be exploited for various functionalities and device applications. Many 2D materials have been fabricated beyond graphene, resulting in a large and rapidly expanding 2D materials family. As a relatively new class of members, 2D molecular crystals (2D MCs) assembled from molecular compounds have been proposed as appealing candidates for next-generation electronic devices, taking advantage of their various salient properties such as being dangling-bond free even in further reduced dimensions (namely, ribbons and dots) and possessing a uniform thickness at the molecular level [1–5]. To date, the discovered 2D MCs have been mainly focused on self-assembled films with complex organic molecules as the building blocks. Notably, the recent fabrication of 2D inorganic molecular crystals (2D IMCs) consisting of tiny inorganic molecules such as Sb_2O_3 has effectively broadened the scope of 2D MCs assembled from compound molecules [6–9]. Given these latest advances, it is naturally intriguing to explore if the 2D IMC class can be further enriched to systems where the building blocks are composed of molecular entities of a single element.

In searching for such 2D IMC systems, we first note that a commonality of the 2D materials derived from single elements from the IIIA to VIA groups is their strong intralayer covalent bonding, such as borophene [10], graphene [11], phosphorene [12], and tellurene [13]. These systems are unlikely to be molecular crystals. On the other hand, the group-VIIA elements may serve as new candidates of 2D IMCs assembled from elementary molecules, taking advantage of their relatively strong intermolecular halogen bonding. To the best of our knowledge, both theoretical and experimental research on the group-VIIA 2D materials is rare. Recently, a few layers of iodine nanosheets have been fabricated by a liquid-phase exfoliation strategy [14], which demonstrate a 2D structure consisting of I_2 molecules. However, the structural properties as well as the intermolecular bonding natures in 2D iodine materials are still not clear. Therefore, the study of the structure-activity relationship of I-based 2D IMCs is of great significance for understanding the intermolecular interactions of 2D IMCs dominated by halogen bonding and promoting their potential applications in molecular physics and optoelectronics.

In this paper, we investigated the structural diversity of I-based monolayers based on *ab initio* calculations combined with global structural searching. We show that 2D monolayered allotropes of I (named iodene) can be stabilized

*zlzhu@zzu.edu.cn
†cuipg@ustc.edu.cn
‡jiayu@zzu.edu.cn

with three distinct structures, namely α-I, β-I, and γ-I, respectively. The intermolecular interactions arising from the halogen bonding play a critical role in the formation of iodene allotropes. Intriguingly, the intermolecular angles between two neighboring I_2 units demonstrate magic angles of 90°, 120°, and 180° for α-, β-, and γ-I, respectively, which serve as a degree of freedom to modulate the structural and electronic properties of iodene monolayers. The γ-I behaves as a quantum spin Hall insulator with a band gap of 0.18 eV, which is a potential topological 2D IMC predicted by theory, and, the 2D allotropes of α-I and β-I are characterized as indirect semiconductors with gaps of 2.30 and 1.94 eV, respectively. These findings bring out candidates of 2D IMCs rooted in the halogen bond, which not only offer different insights into the intermolecular interactions of 2D IMCs, but also will promote their potential applications in molecular physics and optoelectronics.

The paper is organized as follows. In Sec. II, we briefly describe the method and details of the density functional theory (DFT) calculations. In Sec. III, we predict the structural diversity of I-based 2D IMCs dominated by halogen bonding. The electronic properties and topological nature of I-based 2D IMCs are discussed in detail. In Sec. IV, we conclude this work with a brief summary.

II. COMPUTATIONAL DETAILS

Density functional theory (DFT) calculations were performed using the Vienna *ab initio* simulation package (VASP) [15,16]. Particle-swarm optimization (PSO) searches [17] have been carried out to predict the potential 2D structures. The exchange-correlation energy was treated within the projector augmented-wave method [18,19] in the form of Perdew-Burke-Ernzerhof (PBE) [20] with the van der Waals (vdW) corrections of the vdW-DF scheme [21]. The kinetic-energy cutoff for the plane-wave basis set was chosen to be 400 eV. Iodine monolayers were modeled by a periodic 1×1 slab geometry with a vacuum thickness of 20 Å. All structures were fully relaxed until the total energies were converged up to 10^{-4} eV and the Hellmann-Feynman forces were less than 0.01 eV/Å. The band gaps were verified using the nonlocal Heyd-Scuseria-Ernzerhof (HSE06) hybrid functional calculation [22,23]. The phonon calculations employed a supercell approach, as implemented in the PHONOPY code [24]. The maximally localized Wannier functions (MLWFs) were constructed by the WANNIER90 package [25] with the DFT results as inputs, and the Z_2 invariants and edge-state calculations were performed using the WANNIERTOOLS package [25,26].

III. RESULTS AND ANALYSIS

A. Structural diversity and bonding nature of iodene allotropes

Though iodine normally exists in diatomic molecular form, its 3D crystalline structure can be formed with I_2 blocks via intermolecular interaction. As shown in Fig. 1(a), bulk iodine is a layered crystal with an orthorhombic structure (space group *Cmca*) under ambient conditions [27,28] suggesting that the formation of 2D structures with I_2 blocks is feasible. With first-principles calculations combined with global structural searching, we identify three different phases, denoted by

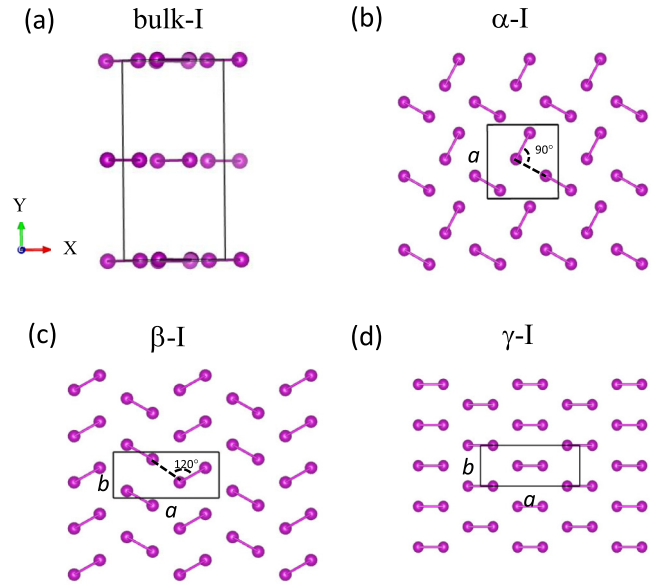

FIG. 1. Atomic structures of bulk iodine and iodene allotropes. (a) Side view of the bulk iodine structure. (b)–(d) Top views of the optimized structures of iodene in different phases: α-I in (b), β-I in (c), and γ-I in (d). Unit cells are indicated by the solid rectangles, and the relative angles between two neighboring I_2 molecules are also indicated.

α-, β-, and γ-I, respectively, as displayed in Figs. 1(b)–1(d). It is found that the β-I phase is derived from a (010) film of the bulk iodine, while the other two allotropes of α- and γ-I exhibit distinctly different structures, with no counterparts in the 3D form. Furthermore, both β- and γ-I have rectangular unit cells, while α-I has a square one.

We first verify the dynamic stabilities of these iodene allotropes by computing their phonon dispersions. As shown in Fig. S1 in the Supplemental Material [29], the vibration spectra of α-, β-, and γ-I have no imaginary frequencies associated with structural instabilities, showing that they are dynamically stable. The thermodynamic stability is further verified by *ab initio* molecular dynamics simulations at a given temperature, up to 5 ps with a time step of 1 fs (see the movies in the Supplemental Material [29]), showing that the equilibrium structures of α-I and β-I can be preserved well at a temperature of 300 K. Expectedly, a lower temperature is required to stabilize the γ-I phase, as it exhibits a tendency of changing into the β phase at a temperature of 200 K.

Different from traditional 2D materials with strong intralayer covalent bonding, the iodene formation is driven by the intermolecular coupling of the halogen-bonded entities. Such an intermolecular coupling is a type of noncovalent interaction, associated with the so-called halogen bonds (XBs). In general, the XB is depicted as $Y\text{-}X\cdots D$, where the three dots represent the bond, X is the electrophilic halogen atom, D is an electron density donor, and Y is typically carbon, nitrogen, or a similar element. In particular, the category of XBs where $Y = X$ [30,31] is related to the crystalline structure of the halogen atoms. The iodine crystal is a prototypical representation of structures stemming from the homo-halogen bonds. We have examined the bond length and nearest atomic

TABLE I. Structural and energetic parameters of iodene allotropes. a, b, and c denote the lattice parameters, and d_{m-m} is the nearest atomic distance between adjacent I_2 molecules. Angle represents the relative angle between two adjacent I_2 molecules, E_b is the binding energy per I_2 molecule, and E_g is the band gap

Structure	a, b (Å)	d_{m-m} (Å)	Angle (deg)	E_b (eV)	E_g (eV)
α-I	$a=b=7.24$	3.47	90	0.85	2.30
β-I	$a=10.04$	3.54	120	0.83	1.94
	$b=4.83$				
γ-I	$a=11.23$	3.60	180	0.72	0.18
	$b=4.54$				
Bulk-I	$a=4.86$	3.55	115	1.12	1.64
	$b=8.02$				
	$c=9.96$				

distance (d_{m-m}) between adjacent I_2 molecules in different allotropes (see Table I), and found that the distances between I_2 molecules are 3.54 and 3.60 Å in β- and γ-I, respectively. Moreover, an unusually short distance of 3.47 Å is observed in α-I. Nevertheless, the distances between adjacent I_2 molecules among the three phases are all significantly shorter than the sum of van der Waals (vdW) radii for the distance of I-I (430 pm). In Fig. S2 of the Supplemental Material [29], the calculated total and differential charge densities further illustrate the distributions of the substantial charge density between adjacent molecules. To quantify the intermolecular coupling strength, the binding energy (E_b) per molecule with respect to an isolated I_2 molecule has been calculated in comparison with that of the bulk iodine, and it is somewhat surprising that the α- and β-I allotropes are almost degenerate in energy, even though their band gaps differ substantially (see more details later).

Obviously, the structural diversity of the iodene allotropes cannot be simply explained by vdW interactions alone. It is necessary to explore the bonding features of different iodene allotropes to reveal the formation mechanism(s) of such 2D IMCs stabilized by halogen bonding. The 3D crystalline iodine demonstrates the highest atomic polarizability in the halogen row because of the largest vdW radius and thus the most evident anisotropy of electrostatic potential on the electron density isosurface [32,33]. In Fig. S2 of the Supplemental Material [29], the calculated charge density differences reveal that the charge distributions of the I_2 molecules in the iodene crystals have changed dramatically compared to that of an isolated molecule. In particular, significant electron depletion and accumulation in the iodenes indicate that there exists local positive and negative charge in the I_2 molecular building blocks. It is not difficult to predict that when two molecules are getting closer, the negative and positive parts will attract each other. Accordingly, the relative orientation between the I_2 units is crucial to the intermolecular coupling. For this reason, we have explored the angles between the orientations of neighboring molecules in these iodene allotropes. The structural parameters and binding energy of each optimized structure are listed in Table I. Intriguingly, the three packing patterns correspond to magic angles of 90°, 120°, and 180°, which are dominated by the halogen bonding. These findings indicate that the intermolecular angle can be exploited as a degree of freedom for depicting and altering the structure of the predicted 2D IMCs.

To explore the interrelationship among the three different phases, we can adjust the intermolecular angle by changing the lattice ratio (a/b) but keeping constant the molecular density in the unit area at 0.04 molecules/Å^2. It is to be noted that the bond length of the I_2 molecule is almost unchanged in the whole process, which is different from the case of applying external stress (see more discussion later). Figure 2 presents the changes in the total energy, as well as the intermolecular angle, as a function of a/b during the phase transitions from α-I to β-I, and further to γ-I. We find that the intermolecular angle remains 90° within the α-I phase, almost unchanged with the lattice ratio in the range of 0.8–1.2. When further increasing the lattice ratio, a phase transition takes place from α-I to β- I, with a kinetic barrier of about 0.08 eV per molecule. Within the broad range of 1.2–2.8, the monolayer preserves the β-I phase, while the intermolecular angle is obtuse, and increases with the lattice ratio. Thereafter, the angle reaches 180° as the lattice ratio approaches 3.0, converting β-I to γ-I. Afterwards, the total energy depicts a parabola form, with the lattice ratio decreasing from 3.0 to 2.2. It passes through the ground state of the γ-I phase with a constant intermolecular angle of 180° in the full pathway. As such, we use the intermolecular angle to depict the iodene allotropes instead of the lattice ratio. In addition, the barrier energy from β- I to γ-I is about 0.26 eV per molecule, and the activation barrier converting γ-I to β- I is 0.13 eV per molecule.

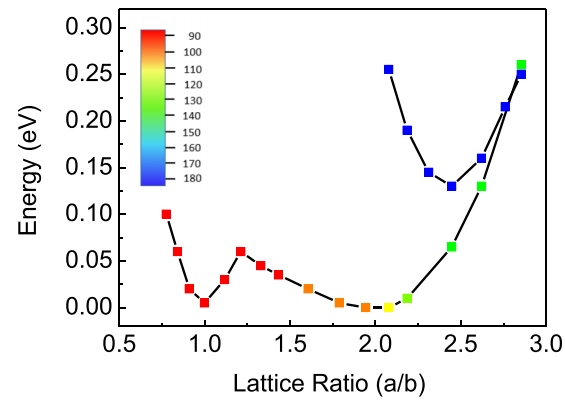

FIG. 2. Total energy as a function of the lattice ratio (a/b) during the transition from α-I to β-I, and to γ-I. The color bar denotes the variation of intermolecular angle from 90° to 180°.

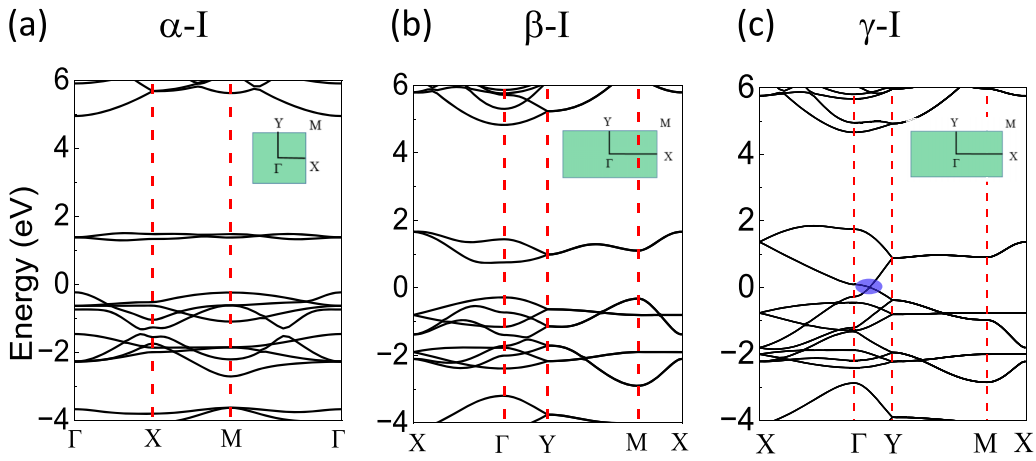

FIG. 3. Band structures of the iodene allotropes for (a) α-I, (b) β-I, and (c) γ-I, obtained within the PBE scheme. The inserts are the corresponding 2D Brillouin zones, and the blue circle in (c) indicates the Dirac cones.

B. Electronic and topological properties of iodenes

To reveal the electronic properties of such iodene allotropes, we calculate their band structures within the Perdew-Burke-Ernzerhof (PBE) functional scheme as shown in Fig. 3. Both α-I and β-I exhibit semiconducting characters with indirect band gaps of $E_g = 1.53$ and 1.07 eV, respectively. It is known that the semilocal PBE scheme may underestimate the band gap. In order to remedy such a potential inaccuracy in the PBE, we perform hybrid density functional theory (DFT) calculations with the HSE06 functional, yielding the corrected $E_g = 2.30$ and 1.94 eV for α-I and β-I, respectively. For comparison, the bulk iodene has an indirect band gap of $E_g = 1.64$ eV within the same computational scheme, indicating that both α-I and β-I have larger band gaps than that of the 3D case. The effective carrier masses of these two 2D IMCs are also calculated. For the squared α-I, the effective masses for electrons and holes are $m_e^* = 0.75m_e$ and $m_h^* = 0.23m_e$, respectively, where m_e is the free-electron rest mass. For the rectangular β-I, $m_{ex}^* = 0.35m_e$, $m_{ey}^* = 0.53m_e$, and $m_{hx}^* = 0.72m_e$, $m_{hy}^* = 2.27m_e$, exhibiting significant carrier anisotropies.

As explicitly illustrated in Fig. 3(c) for the γ-I, the band structure exhibits Dirac cones around the Fermi level in the Brillouin zone (BZ) along the Γ-Y direction, potentially signifying its nontrivial topological property. The corresponding orbital-projected band structures without and with spin-orbit coupling (SOC) are further contrasted in Figs. 4(a) and 4(b). Without SOC, the Dirac cones have a small band gap of 21 meV [see the inset of Fig. 4(a)], with an intrinsic band inversion according to the orbital contributions. With the inclusion of SOC, the band gap is enlarged to 0.18 eV, while the band orders are kept [Fig. 4(b)]. To quantitatively verify the topological nature of γ-I, we have adopted the WANNIER90 code combined with VASP to calculate the corresponding topological invariant Z_2 based on the band structure with SOC. We obtain $Z_2 = 1$, which unambiguously characterizes γ-I to be a quantum spin Hall (QSH) insulator. Here, it is noted that the strong SOC originating from the iodine element can expand the inverted band gap drastically to 0.18 eV, which is significantly larger than k_BT (~26 meV), suggesting that the QSH effect can be realized at room temperature or higher.

As another manifestation of the nontrivial topological nature, the topologically protected nontrivial edge states for γ-I along different directions are also calculated and verified, as shown in Figs. 4(c), and 4(d).

To further understand the structure-activity relationship of such iodene allotropes, we first examine the electronic property variations during structural evolution, as presented in Fig. 5(a). We observe that the band gap of α-I decreases with an increased lattice ratio, but maintains an intermolecular angle of 90° with little fluctuation. On the other hand, the β-I phase adopts flexible intermolecular angles of $90° < \theta < 120°$, and the band gap does not change much in such an angle range. Not until the intermolecular angle is larger than 120°, does the band gap decrease sharply, leading to the phase transition from β-I to γ-I. The tuning behaviors of the band

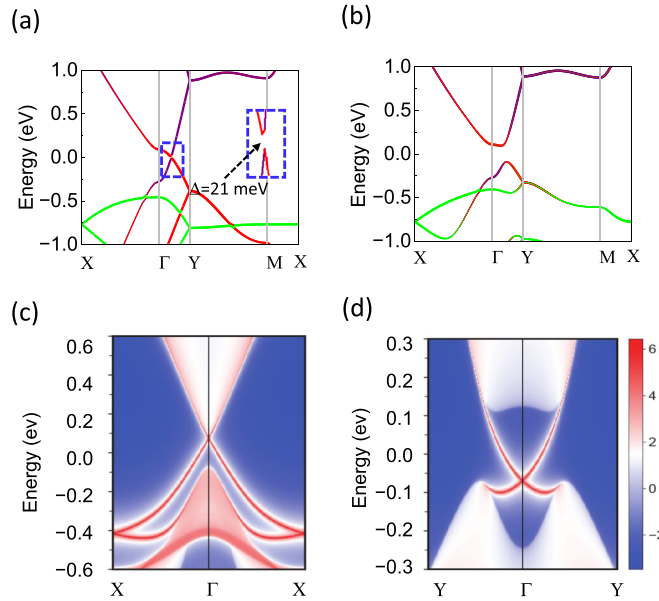

FIG. 4. Band structures of γ-I (a) without and (b) with the SOC. The purple, red, and green data points denote the spectral weights contributed by the p_x, p_y, and p_z orbitals of the I atoms, respectively. (c), (d) Edge states of the semi-infinite slab along the [010] and [100] directions, respectively.

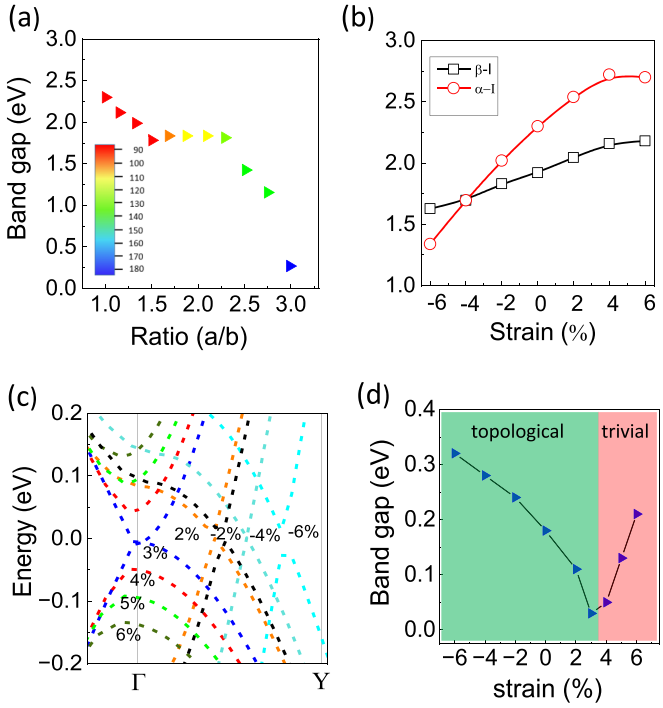

FIG. 5. (a) Band-gap fluctuation during the structural evolution from α-I to β-I, and to γ-I. The color bar denotes the intermolecular angles change from 90° to 180°. (b) Band gap as a function of biaxial strain for α-I and β-I. (c) Band structures of γ-I without SOC under external strains (ε from -6% to 6%) obtained within the PBE scheme. (d) Band-gap variation with external strains for γ-I with SOC. The green and red areas indicate the topologically nontrivial and trivial regions under the strain, respectively.

gaps for α-I and γ-I can be mainly attributed to the strain induced by the variable lattice ratio, while for β-I the tuning is attributable to the variable intermolecular angles and the residual stresses. Next, we investigate the more direct in-plane biaxial strain effects on the electronic properties of these iodene allotropes. Figure 5(b) shows the band-gap variations with the biaxial strain (ε) from -6% to 6% for α-I and β-I. The results suggest that α-I is sensitive to external strains, and the band gap can be effectively tuned in a wide range of 1.34–2.72 eV accordingly. In contrast, the band gap of β-I does not change drastically under applied external strains, similar as observed for varying the lattice ratio. Such insensitive responses to the strain are tied to the flexible structure and changeable intermolecular angle of β-I.

As for γ-I, it is of significance to investigate the strain effects on the topological properties. Given that the band of γ-I without SOC possesses a gap of 21 meV, we first calculate the evolution of the band structures with an external biaxial strain without the SOC, as displayed in Fig. 5(c). Intriguingly, this band gap decreases upon applying a small tensile or compressive strain, and is to be closed under a tensile strain of $\varepsilon = 3\%$ or compressive stress of $\varepsilon = -2\%$. Beyond the two critical values, the stresses reopen the band gaps. To determine the strain effects on the topological properties, we further perform the band-structure calculations including SOC and calculate the corresponding topological invariants for the strained γ-I structures. The results indicate that the nontrivial topology of the γ-I phase is rather robust under compressive strain ($\varepsilon = -6\%$–0%), all showing $Z_2 = 1$. In contrast, the topologically nontrivial properties of γ-I are only maintained under a tensile strain of $0 < \varepsilon \leqslant 3\%$, and larger tensile strains (e.g., $\varepsilon =$ 4%–6%) result in the transition from a QSH to a trivial semiconductor ($Z_2 = 0$). Figure 5(d) presents the band-gap evolution with external strain with the inclusion of SOC. It is found that the nontrivial band gap can be effectively tuned from 0.03 to 0.32 eV under external strains ($\varepsilon = -6\%$ to 3%), while the tensile strains ($\varepsilon = 4\%$–6%) result in trivial band gaps varying from 0.05 to 0.21 eV. These results illustrate that the QSH states of γ-I can be effectively tuned by external strain.

IV. DISCUSSION AND CONCLUSIONS

Before closing, we briefly discuss the experimental feasibility and potential applications of such 2D IMCs. The fabricated iodine nanosheets by using a liquid-phase exfoliation strategy [14] demonstrate the proposed β-I structure. It is expected to realize our predicted iodene allotropes through more precise growth controlling, for example, by epitaxial growth on a suitable substrate. In addition, the 2D IMCs also provide promising potential applications in electronic and optoelectronics devices due to their unique structures and properties. For example, the 2D IMC film of Sb_2O_3 was recently used as a substrate in MoS_2-based field-effect transistors, leading to a higher mobility and higher stability of the device performance due to the fewer charge scattering centers and trap states than conventional SiO_2 [7]. Taking advantage of the structural diversity and interesting properties, our predicted iodene allotropes may also be used as vdW dielectric materials in fabricating high-performance 2D devices. Furthermore, high-order vdW heterostructural superlattices can be envisioned by rolling up vdW heterostructures with technological applications [34,35]. In this context, the 2D IMCs predicted here can be used as intercalated molecules, but in a highly ordered form.

In conclusion, we have predicted the structural diversity of I-based monolayers based on *ab initio* calculations combined with global structural searching. These 2D IMCs assembled from elementary I_2 molecules can be stabilized with distinct structures of α-I, β-I, and γ-I phases. The intermolecular interactions arising from the halogen bonding play a critical role in the formation of such iodene allotropes. We also revealed that the intermolecular angle between two neighboring I_2 units serves as a degree of freedom in modulating the structural and electronic properties of the iodenes, with magic angles of 90°, 120°, and 180° and band gaps of 2.30, 1.94, and 0.18 eV for α-, β-, and γ-I, respectively. Furthermore, the γ phase behaves as a QSH insulator with tunable topological properties, which offers a candidate for potential topological 2D IMCs. These findings substantially enrich our understanding of 2D IMCs based on halogen bonding, and the salient properties of such 2D IMCs can be exploited as integrated components in various future electronic devices based on 2D materials.

ACKNOWLEDGMENTS

This work was supported by the National Natural Science Foundation of China (Grants No. 12274375, No. 12074099, and No. 11974323), the Natural Science Foundation of Henan

Province of China (Grants No. 212300410409), the Innovation Program for Quantum Science and Technology (No. 2021ZD0302800), the Strategic Priority Research Program of Chinese Academy of Sciences (Grant No. XDB30000000), and the Anhui Initiative in Quantum Information Technologies (Grants No. AHY170000). All calculations were performed at Zhengzhou National Supercomputing Center, Zhengzhou University.

[1] N. Clement and A. Fujiwara, Nat. Nanotechnol. **12**, 725 (2017).
[2] X. P. Chen, M. Roemer, L. Yuan, W. Du, D. Thompson, E. del Barco, and C. A. Nijhuis, Nat. Nanotechnol. **12**, 797 (2017).
[3] L. J. Cui, R. J. Miao, K. Wang, D. Thompson, L. A. Zotti, J. C. Cuevas, E. Meyhofer, and P. Reddy, Nat. Nanotechnol. **13**, 122 (2018).
[4] M. Cinchetti, V. A. Dediu, and L. E. Hueso, Nat. Mater. **16**, 507 (2017).
[5] H. Atesci, V. Kaliginedi, J. A. C. Gil, H. Ozawa, J. M. Thijssen, P. Broekmann, M. A. Haga, and S. J. van der Molen, Nat. Nanotechnol. **13**, 117 (2018).
[6] W. Han, P. Huang, L. Li, F. K. Wang, P. Luo, K. L. Liu, X. Zhou, H. Q. Li, X. W. Zhang, Y. Cui, and T. Y. Zhai, Nat. Commun. **10**, 4728 (2019).
[7] K. L. Liu, B. Fin, W. Han, X. Chen, P. L. Gong, L. Huang, Y. H. Zhao, L. Li, S. J. Yang, X. Z. Hu, J. Y. Duan, L. X. Liu, F. K. Wang, F. W. Zhuge, and T. Y. Zhai, Nat. Electron. **4**, 906 (2021).
[8] X. Feng, X. L. Peng, B. X. Peng, Z. X. Li, W. T. Huang, S. J. Yang, K. Pei, Z. D. Sun, F. Q. Huang, H. Q. Li, Z. G. Shuai, and T. Y. Zhai, J. Am. Chem. Soc. **143**, 20192 (2021).
[9] K. L. Liu, L. X. Liu, and T. Y. Zhai, J. Phys. Chem. Lett. **13**, 2173 (2022).
[10] A. J. Mannix, X. F. Zhou, B. Kiraly, J. D. Wood, D. Alducin, B. D. Myers, X. L. Liu, B. L. Fisher, U. Santiago, J. R. Guest, M. J. Yacaman, A. Ponce, A. R. Oganov, M. C. Hersam, and N. P. Guisinger, Science **350**, 1513 (2015).
[11] K. S. Novoselov, A. K. Geim, S. V. Morozov, D. Jiang, Y. Zhang, S. V. Dubonos, I. V. Grigorieva, and A. A. Firsov, Science **306**, 666 (2004).
[12] L. K. Li, Y. J. Yu, G. J. Ye, Q. Q. Ge, X. D. Ou, H. Wu, D. L. Feng, X. H. Chen, and Y. B. Zhang, Nat. Nanotechnol. **9**, 372 (2014).
[13] Z. L. Zhu, X. L. Cai, S. H. Yi, J. L. Chen, Y. W. Dai, C. Y. Niu, Z. X. Guo, M. H. Xie, F. Liu, J. H. Cho, Y. Jia, and Z. Y. Zhang, Phys. Rev. Lett. **119**, 106101 (2017).
[14] M. Qian, Z. Xu, Z. Wang, B. Wei, H. Wang, S. Hu, L. M. Liu, and L. Guo, Adv. Mater. **32**, 2004835 (2020).
[15] G. Kresse and J. Furthmuller, Comput. Mater. Sci. **6**, 15 (1996).
[16] G. Kresse and J. Furthmuller, Phys. Rev. B **54**, 11169 (1996).
[17] Y. C. Wang, J. A. Lv, L. Zhu, and Y. M. Ma, Phys. Rev. B **82**, 094116 (2010).
[18] P. E. Blochl, Phys. Rev. B **50**, 17953 (1994).
[19] G. Kresse and D. Joubert, Phys. Rev. B **59**, 1758 (1999).
[20] J. P. Perdew, K. Burke, and M. Ernzerhof, Phys. Rev. Lett. **77**, 3865 (1996).
[21] M. Dion, H. Rydberg, E. Schröder, D. C. Langreth, and B. I. Lundqvist, Phys. Rev. Lett. **92**, 246401 (2004).
[22] J. Heyd, G. E. Scuseria, and M. Ernzerhof, J. Chem. Phys. **118**, 8207 (2003).
[23] O. A. Vydrov, J. Heyd, A. V. Krukau, and G. E. Scuseria, J. Chem. Phys. **125**, 074106 (2006).
[24] A. Togo, F. Oba, and I. Tanaka, Phys. Rev. B **78**, 134106 (2008).
[25] A. A. Mostofi, J. R. Yates, Y.-S. Lee, I. Souza, D. Vanderbilt, and N. Marzari, Comput. Phys. Commun. **178**, 685 (2008).
[26] Q. Wu, S. Zhang, H.-F. Song, M. Troyer, and A. A. Soluyanov, Comput. Phys. Commun. **224**, 405 (2018).
[27] F. V. Bolhuis, P. Koster, and T. Migchelsen, Acta Crystallogr. **23**, 90 (1967).
[28] K. Sasvári, Acta Crystallogr, Sect. B **31**, 334 (1975).
[29] See Supplemental Material at http://link.aps.org/supplemental/10.1103/PhysRevB.108.115409 for details regarding the phonon spectra, charge densities, and molecular dynamics simulations of the structural stability of iodene allotropes.
[30] G. R. Desiraju, P. S. Ho, L. Kloo, A. C. Legon, R. Marquardt, P. Metrangolo, P. Politzer, G. Resnati, and K. Rissanen, Pure Appl. Chem. **85**, 1711 (2013).
[31] Y. He, J. Zhang, L. Lei, and W. Kong, Angew. Chem., Int. Ed. **56**, 3541 (2017).
[32] P. Politzer, P. Lane, M. C. Concha, and M. Murray, J. Mol. Model. **13**, 305 (2007).
[33] P. Politzer, J. S. Murray, and T. Clark, Phys. Chem. Chem. Phys. **12**, 7748 (2010).
[34] B. Zhao, Z. Wan, Y. Liu, J. Xu, X. Yang, D. Shen, Z. Zhang, C. Guo, Q. Qian, J. Li, R. Wu, Z. Lin, X. Yan, B. Li, Z. Zhang, H. Ma, B. Li, X. Chen, Y. Qiao, I. Shakir *et al.*, Nature (London) **591**, 385 (2021).
[35] Z. Lin, Z. Wan, F. Song, B. Huang, C. Jia, Q. Qian, J. S. Kang, Y. Wu, X. Yan, L. Peng, C. Wan, J. Zhou, Z. Sofer, I. Shakir, Z. Almutairi, S. Tolbert, X. Pan, Y. Hu, Y. Huang, and X. Duan, Chem **7**, 1887 (2021).